



Whole-Tumor Histogram Analysis of Multiple Diffusion Metrics for Glioma Genotyping

Ankang Gao, MD • Huiting Zhang, PhD • Xu Yan, PhD • Shaoyu Wang, PhD • Qianqian Chen, MD • Eryuan Gao, BM • Jinbo Qi, BM • Jie Bai, MD • Yong Zhang, PhD • Jingliang Cheng, PhD

From the Department of MRI, the First Affiliated Hospital of Zhengzhou University, Zhengzhou, China (A.G., Q.C., E.G., J.Q., J.B., Y.Z., J.C.); and Department of MR Scientific Marketing, Siemens Healthineers, Shanghai, China (H.Z., X.Y., S.W.). Received April 5, 2021; revision requested June 22; revision received September 15; accepted October 11. **Address correspondence to** J.C. (e-mail: fccchengjl@zzu.edu.cn).

J.C. supported by the National Key R&D Program of China (2016YFC0106900). J.B. supported by Medical Tackling Problems in Science and Technology Plain Program of Henan Province, China (201702070).

Conflicts of interest are listed at the end of this article.

Radiology 2022; 302:652–661 • <https://doi.org/10.1148/radiol.210820> • Content codes:  

Background: The isocitrate dehydrogenase (*IDH*) genotype and *1p/19q* codeletion status are key molecular markers included in glioma pathologic diagnosis. Advanced diffusion models provide additional microstructural information.

Purpose: To compare the diagnostic performance of histogram features of multiple diffusion metrics in predicting glioma *IDH* and *1p/19q* genotyping.

Materials and Methods: In this prospective study, participants were enrolled from December 2018 to December 2020. Diffusion-weighted imaging was performed by using a spin-echo echo-planar imaging sequence with five *b* values (500, 1000, 1500, 2000, and 2500 sec/mm²) in 30 directions for every *b* value and one *b* value of 0. Diffusion metrics of diffusion-tensor imaging (DTI), diffusion-kurtosis imaging (DKI), neurite orientation dispersion and density imaging (NODDI), and mean apparent propagator (MAP) were calculated, and their histogram features were analyzed in regions that included the entire tumor and peritumoral edema. Comparisons between groups were performed according to *IDH* genotype and *1p/19q* codeletion status. Logistic regression analysis was used to predict the *IDH* and *1p/19q* genotypes.

Results: A total of 215 participants (115 men, 100 women; mean age, 48 years \pm 13 [standard deviation]) with grade II (*n* = 68), grade III (*n* = 35), and grade IV (*n* = 112) glioma were included. Among the DTI, DKI, NODDI, MAP, and total diffusion models, there were no significant differences in the areas under the receiver operating characteristic curve (AUCs) for predicting *IDH* mutations (AUC, 0.76, 0.82, 0.78, 0.81, and 0.82, respectively; *P* > .05) and *1p/19q* codeletion in gliomas with *IDH* mutations (AUC, 0.83, 0.81, 0.82, 0.83, and 0.88, respectively; *P* > .05). A regression model with an *R*² value of 0.84 was used for the Ki-67 labeling index and histogram features of the diffusion metrics.

Conclusion: Whole-tumor histogram analysis of multiple diffusion metrics is a promising approach for glioma isocitrate dehydrogenase and *1p/19q* genotyping, and the performance of diffusion-tensor imaging is similar to that of advanced diffusion models.

Clinical trial registration no. ChiCTR2100048119

© RSNA, 2021

Online supplemental material is available for this article.

An earlier incorrect version appeared online. This article was corrected on December 14, 2021.

In the 2016 World Health Organization (WHO) classification of tumors for the central nervous system (1), glioma genotyping instead of grading was considered the most relevant information for neuroradiologists. The isocitrate dehydrogenase (*IDH*) genotype and *1p/19q* codeletion status are two essential molecular markers that divide glioma into three groups: *IDH* wild-type, *IDH* mutant with *1p/19q* non-codeletion, and *IDH* mutant with *1p/19q* codeletion (2). This molecular marker grouping method is suitable for low-grade glioma (LGG) (3), and it has an important role in clarifying the biologic characteristics of LGG, predicting prognosis, and planning treatment (4,5). Thus, useful noninvasive imaging markers of *IDH* mutational status have important clinical value for patients with LGG.

MRI is an essential preoperative examination for patients with glioma. Diffusion, perfusion, and metabolic imaging have been used extensively in glioma genotyping

research (6–11). The use of diffusion-weighted MRI has increased in recent years because it does not require contrast material, it enables quantitative assessment of the whole tumor microstructure at a relatively high spatial resolution, and it is easily accessible. Diffusion-tensor imaging (DTI) metrics, such as the mean diffusivity and fractional anisotropy (6,9,12), and diffusion-kurtosis imaging (DKI) (13,14) metrics, such as the mean kurtosis, have been reported to provide insight into *IDH* mutational status. The application of neurite orientation dispersion and density imaging (NODDI) metrics for depicting LGG *IDH* status is controversial (9,15). When determining the *1p/19q* codeletion status of *IDH* mutations in LGG, the diagnostic efficacy of fractional anisotropy has been shown to be inconsistent in various studies (6,12,16), and NODDI metrics are not considered useful (9). Meanwhile, mean apparent propagator (MAP) MRI, a diffusion-weighted MRI framework to

Abbreviations

AUC = area under the receiver operating characteristic curve, DKI = diffusion-kurtosis imaging, DTI = diffusion-tensor imaging, ICVF = intracellular volume fraction, LGG = low-grade glioma, MAP = mean apparent propagator, NODDI = neurite orientation dispersion and density imaging, WHO = World Health Organization

Summary

Although advanced diffusion MRI depicts more microstructural changes than other approaches, performance in glioma isocitrate dehydrogenase and *1p/19q* genotyping is equal to that of diffusion-tensor imaging.

Key Results

- In a prospective study of 215 participants with glioma grades II–IV, diffusion-tensor MRI had moderate to good diagnostic performance for identifying glioma isocitrate dehydrogenase (*IDH*; area under the receiver operating characteristic curve [AUC], 0.76) and *1p/19q* (AUC, 0.83) genotypes.
- The performance of diffusion-kurtosis imaging, neurite orientation dispersion and density imaging, and mean apparent propagator models for *IDH* and *1p/19q* genotypes was similar to that of diffusion-tensor MRI (all comparisons, $P > .05$).

help accurately characterize and quantify anisotropic diffusion properties at various levels of diffusion sensitivity (17,18), has been used in glioma differential diagnostic research (19). However, there are neither any reports on the role of MAP MRI in glioma genotyping nor, to our knowledge, any studies comparing the DTI, DKI, NODDI, and MAP diffusion models for distinguishing glioma *IDH* and *1p/19q* genotypes. Thus, the purpose of our study was to compare the diagnostic accuracy of DTI, DKI, NODDI, and MAP metrics combined with histogram analysis, which could be acquired within a single scan, for predicting *IDH* genotypes and *1p/19q* codeletion in WHO grade II and III gliomas, and to assess the application of MAP in glioma grading.

Materials and Methods

Three authors (H.Z., X.Y., and S.W.) are employees of Siemens Healthineers and worked as MRI research scientists to provide technical support for this study under Siemens' collaboration regulation without any payment or personal concern regarding the study. One author (J.C.) controlled the data and the information submitted for publication.

Study Participants

The ethics committee of our hospital approved this prospective study (www.chictr.org.cn: ChiCTR2100048119), and all the participants provided written informed consent. Data generated by the authors or analyzed during the study are available at <http://www.medresman.org>. Participants diagnosed with glioma before the first surgical resection at our institution between December 2018 and December 2020 were selected. The inclusion criteria were as follows: age between 17 and 75 years, diffusion-weighted MRI performed less than 2 weeks before surgery and antitumor therapy initiation, and definite histopathologic diagnosis of glioma on the basis of the WHO 2016 classification criteria. The exclusion criteria were a diagnosis

Inclusion criteria (n=404)

- 1) Patients' age range 17–75 years, have not yet undergone antitumor therapy
- 2) MRI with diffusion was performed less than 2 weeks before surgery
- 3) Definite histopathologic diagnosis of glioma based on the WHO 2016 classification criteria.

Patients excluded (n=189)

WHO I gliomas (n=3), ependymomas (n=7), metastases (n=25), and other nonglial brain tumors (n=154).

Patients included (n=215)

Figure 1: Participant selection flowchart. WHO = World Health Organization.

of WHO grade I gliomas and ependymomas, metastases, and other nonglial brain tumors. An overview of the case selection process is in Figure 1.

The participants were first grouped according to *IDH* genotype (ie, the wild-type and mutation groups). Subsequently, the WHO grade II and III glioma *IDH* mutation group was further divided according to the *1p/19q* phenotype.

MRI Parameters

Participants underwent diffusion-weighted imaging and conventional MRI with a 3.0-T scanner (Magnetom Prisma; Siemens Healthcare) with a 64-channel head-neck coil. Diffusion-weighted imaging was performed by using a spin-echo echo-planar imaging sequence with the following parameters: field of view, 220×220 mm²; section thickness, 2.2 mm; 60 sections; TR msec/TE msec, 2500/71; five *b* values (500, 1000, 1500, 2000, and 2500 sec/mm²) with diffusion encoding in 30 directions for every *b* value, and one *b* value of 0 sec/mm². Axial T2-weighted fast spin echo (3800/92) and T2-weighted fast inversion recovery magnitude and dark-fluid imaging parameters were as follows: 8000/81; 256×256 pixel matrix and a 240×240 mm² field of view, with a 5-mm section thickness and a 1-mm intersection gap. Finally, sagittal three-dimensional T1-weighted magnetization-prepared rapid gradient echo imaging was performed with the following parameters: 2300/2.32; 256×256 matrix; 240×240 mm field of view; and section thickness, 0.9 mm.

Image Processing

DTI, DKI, MAP, and NODDI metrics (Table E1 [online]) were calculated by using an in-house postprocessing software (NeuDiLab) based on the open-resource tool DIPY (Diffusion Imaging in Python, <https://dipy.org>) (19,20) and Amico (20) (<https://github.com/daducci/AMICO>). Histogram analysis was performed by using the open-resource tool pyradiomics (ver-

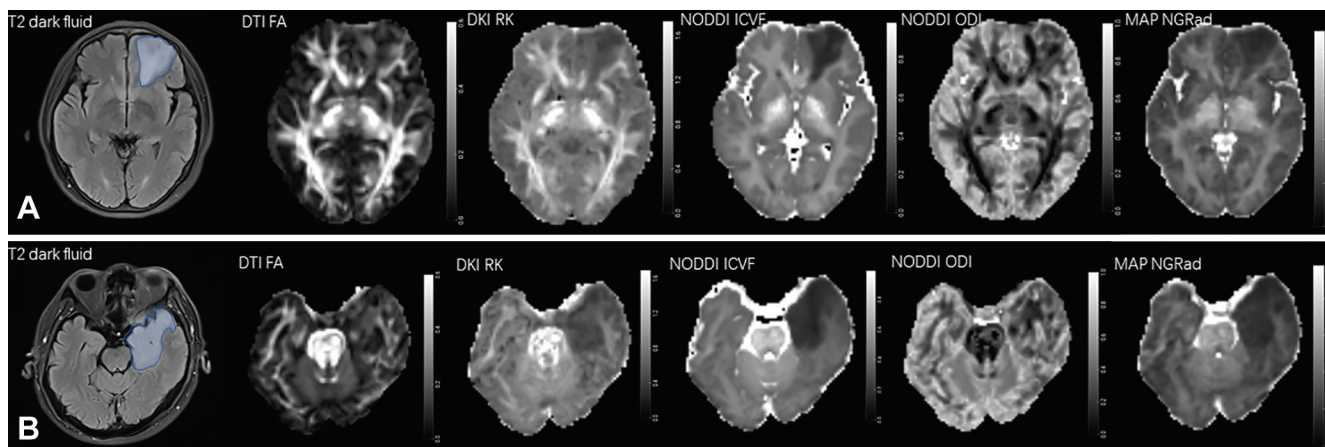


Figure 2: The blue lines on the T2-weighted dark fluid images show the lesions included in the volume of interest. **(A)** Images in a 52-year-old woman with World Health Organization (WHO) grade II oligodendroglioma with isocitrate dehydrogenase (*IDH*) mutation type and *1p/19q* codeletion. **(B)** Images in a 52-year-old man with WHO grade II astrocytoma with *IDH* wild-type and *1p/19q* non-codeletion. DKI = diffusion-kurtosis imaging, DTI = diffusion-tensor imaging, FA = fractional anisotropy, ICVF = intracellular volume fraction, MAP = mean apparent propagator, NGRad = radial non-Gaussianity, NODDI = neurite orientation dispersion and density imaging, ODI = orientation dispersion index, RK = radial kurtosis.

sion 3.0.1, <https://github.com/AIM-Harvard/pyradiomics>); the histogram features of this tool are defined in Table E2 (online). The volume of interest was manually drawn around the entire tumor and peritumoral edema on axial T2-weighted fast-inversion-recovery magnitude and dark fluid images (Fig 2) in all the participants by consensus between a neuroradiologist (J.B., with 20 years of experience in neuroradiology) and a PhD candidate in imaging medicine (A.G., with 5 years of experience in neuro-oncology). The volume of interest was spatially transferred to the corresponding diffusion parameters by nonlinear transformation between the T2-weighted and the diffusion image with a *b* value of 0 sec/mm² by using Elastix (<https://elastix.lumc.nl/>).

Molecular Studies

IDH1/2 mutations in the hotspot codons *R132* and *R172* on the excised surgical specimens were determined by Sanger sequencing, and a mutation in any one of them was diagnosed as an *IDH* mutation. The *1p/19q* deletions were detected at fluorescence in situ hybridization analysis. The *1p/19q* codeletion was defined as a signal ratio of *1p/19q* less than 0.70, and *19q/19p* less than 0.70. The Ki-67 labeling index was determined by using immunohistochemistry.

Statistical Analysis

The univariate distributions of the metric variables are expressed as means \pm standard deviation. A two-tailed Mann-Whitney *U* test was used for all two-group comparisons, and the Kruskal-Wallis test was used for multiple-group comparisons. Receiver operating characteristic curve analyses were also undertaken to assess the diagnostic performance. Statistical analysis was performed by using software (SPSS, version 19.0; IBM), and two-sided *P* values less than .05 were considered to indicate statistical significance.

The features from the histogram of the DTI, DKI, MAP, and NODDI metrics, showing *P* values less than .001 in the

identification of the *IDH* and *1p/19q* genotypes, were selected to set up logistic regression models for each individual and total diffusion model. We used Bonferroni correction for multi-parameter model *P* values corrected for multiple comparisons. McNemar test was used to assess differences between model performances in predicting the *IDH* and *1p/19q* genotypes. Receiver operating characteristic curve analysis was performed for all comparisons. DeLong test was used to observe the difference in the area under the receiver operating characteristic curve (AUC) for the models. Software (R, version 3.6.1; R Foundation for Statistical Computing) was used to set up and compare the models.

The correlations between the Ki-67 labeling index and each diffusion metric and correlations among all diffusion metrics were evaluated by using the Pearson correlation coefficient. A multiple linear regression between Ki-67 labeling index and the diffusion metrics histogram features was performed.

Results

Participant Demographics

Overall, 215 participants (115 men, 100 women; mean age, 48 years \pm 13; age range, 22–70 years) were included in this study. According to the histologic classification, 68 participants were diagnosed with WHO grade II glioma (50 astrocytomas, 18 oligodendrogliomas), 35 participants were diagnosed with WHO grade III glioma (14 astrocytomas, 21 oligodendrogliomas), and 112 participants were diagnosed with WHO grade IV glioblastoma multiforme. *IDH* gene mutations were identified in 54 of 68 grade II gliomas, 24 of 35 grade III gliomas, and nine of 112 grade IV gliomas. An overview of the participant stratification according to *IDH* and *1p/19q* status is shown in Table 1. Some results from some of the participants were exhibited on two digital posters (Appendix E1 [online]) at the annual meeting of the International Society for Magnetic Resonance in Medicine 2021 (<https://www.ismrm.org/21ml/>).

Table 1: Participant Demographics

Parameter	All Glioma Subtypes	IDH Wild-Type	IDH Mutation
No. of participants	215	128	87
Mean age and SD (y)	48 ± 13 (17–74)	52 ± 13 (17–74)	43 ± 11 (17–66)
Male participants	115	69	46
Female participants	100	59	41
WHO grade II	68	14	54
1p/19q codeletion	20
Non-codeletion	29
NOS	5
WHO grade III	35	11	24
1p/19q codeletion	19
Non-codeletion	3
NOS	2
Oligodendroglioma	39	0	39
1p/19q codeletion	39
Non-codeletion	0
NOS	0
Astrocytoma	64	25	39
1p/19q codeletion	0
Non-codeletion	32
NOS	7
Glioblastoma	112	103	9

Note.—Unless otherwise indicated, data are the number of participants. Data in parentheses are ranges. IDH = isocitrate dehydrogenase, NOS = not otherwise specified, WHO = World Health Organization.

Correlation of Diffusion MRI Metrics with IDH and 1p/19q Genotype in LGG

Several metrics of histogram features could be used to classify the glioma IDH genotypes and identify the 1p/19q genotypes of IDH mutations in gliomas simultaneously; these features have been identified in Table E3A (online). Figure 3 shows five of them with a representative distribution in the IDH wild-type, IDH mutation with 1p/19q codeletion, and IDH mutation with 1p/19q non-codeletion groups.

The root mean square fractional anisotropy of DTI, the 10th percentile radial kurtosis of DKI, the 10th percentile intracellular volume fraction of NODDI, and the 10th percentile radial non-Gaussianity of MAP were the most useful metrics in the single diffusion model logistic regression analysis for predicting the IDH mutation type (Table 2). Moreover, the metrics were significantly higher in gliomas with IDH mutations than in IDH wild-type gliomas (Fig 4A). In the combined diffusion model, the logistic regression analysis showed that 10th percentile radial kurtosis of DKI was the most useful metric for IDH genotyping.

The median radial diffusivity of DTI, 10th percentile intracellular volume fraction of NODDI, and the robust mean absolute deviation orientation dispersion index of NODDI were more useful in the single diffusion model logistic regression analysis for predicting 1p/19q codeletion in gliomas with IDH mutations (Table 2). Median radial diffusivity of DTI was significantly higher, but 10th percentile intracellular volume fraction of NODDI and

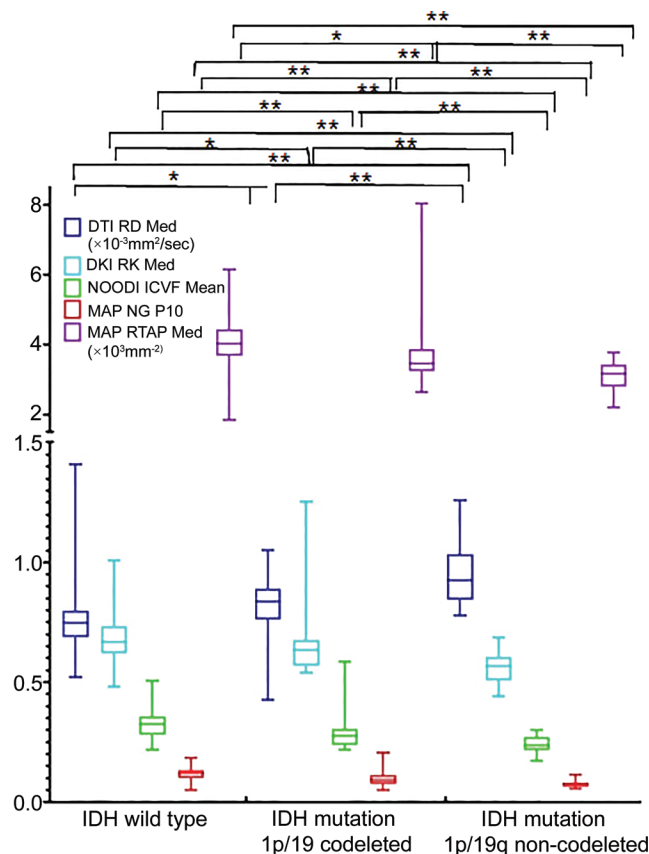


Figure 3: Plots show the distribution of metrics that could be used to detect the isocitrate dehydrogenase (IDH) and 1p/19q genotypes simultaneously ($P < .001$) in the IDH wild-type, IDH mutation with 1p/19q codeletion, and IDH mutation with 1p/19q non-codeletion groups. DKI = diffusion-kurtosis imaging, DTI = diffusion-tensor imaging, ICVF = intracellular volume fraction, MAP = mean apparent propagator, med = median, NG = non-Gaussianity, NODDI = neurite orientation dispersion and density imaging, P10 = 10th percentile, RD = radial diffusivity, RK = radial kurtosis, RTAP = return to the axis probability. * $P = .001-.05$, ** $P \leq .001$.

robust mean absolute deviation orientation dispersion index of NODDI were significantly lower in grade II and III gliomas with IDH mutation and 1p/19q codeletion than in those with 1p/19q non-codeletion (Fig 4B). In the combined diffusion model, the logistic regression analysis showed that the 90th percentile orientation dispersion index of NODDI was more useful than the other metrics in predicting 1p/19q codeletion.

We found no evidence of a difference in the AUC (Fig 5) and accuracy (Table 3) between the single and combined diffusion logistic models for predicting IDH genotyping and IDH mutation glioma 1p/19q genotyping ($P > .05$). The AUC, accuracy, sensitivity and specificity values, and optimal threshold for useful metrics for predicting IDH genotyping and IDH mutation glioma 1p/19q genotyping are reported in Table 4.

Correlation of Diffusion MRI Metrics with IDH Genotypes in Glioblastoma Multiforme

Because of the large difference in the sample size between the IDH mutation and wild-type groups in glioblastoma multiforme in this research, we included only diffusion MRI metrics with significant differences ($P < .05$) between the two groups

Table 2: Logistic Regression Models in the Prediction of IDH and 1p/19q Genotype Grade II and III Gliomas

Model	β Level	Corrected <i>P</i> Value*	AUC†	Accuracy (%)‡
<i>IDH</i> mutation vs <i>IDH</i> wild-type				
DTI model			0.76 (0.64, 0.88)	82 (84/103)
Intercept	2.31	>.99		
DTI FA RMS	−17.9	.04		
DTI MD RMS	3.09	.33		
DKI model			0.82 (0.73, 0.92)	80 (82/103)
Intercept	10.25	.62		
DKI FA P90	−9.77	.69		
DKI MD median	−1.41	>.99		
DKI RD P10	3.01	>.99		
DKI RK P10	−13.67	.03		
NODDI model			0.78 (0.67, 0.91)	78 (80/103)
Intercept	5.83	.001		
NODDI ICVF P90	−6.35	.34		
NODDI ICVF P10	−11.85	.10		
MAP model			0.81 (0.70, 0.91)	81 (83/103)
Intercept	8.08	.02		
MAP NGRad P10	−71.01	.05		
MAP QIV mean	−0.01	>.99		
MAP RTAP P90	−0.48	.79		
Combined model			0.82 (0.73, 0.92)	81 (83/103)
Intercept	11.19	>.99		
DKI FA P90	−10.08	.74		
DKI RD median	−1.41	>.99		
DKI RD P10	2.35	>.99		
DKI RK P10	−13.46	.05		
MAP NGRad P90	−5.06	>.99		
<i>IDH</i> -mutant 1p/19q codeletion vs <i>IDH</i> -mutant 1p/19q non-codeletion				
DTI model			0.83 (0.74, 0.93)	77 (55/71)
Intercept	7.74	.04		
DTI AD IR	−2.35	>.99		
DTI AD kurtosis	0.4	.56		
DTI RD median	−9.05	.03		
DKI model			0.81 (0.71, 0.91)	70 (50/71)
Intercept	−11.21	.1		
DKI AD skewness	0.28	>.99		
DKI AK RMS	15.74	.85		
DKI MD IR	−0.97	>.99		
DKI MD kurtosis	0.19	>.99		
DKI RK P10	5.34	>.99		
NODDI model			0.82 (0.73, 0.92)	77 (55/71)
Intercept	−8.11	.0005		
NODDI ICVF P10	27.977	.01		
NODDI ODI rMAD	53.43	.01		
MAP model			0.83 (0.74, 0.93)	77 (55/71)
Intercept	−4.78	.32		
MAP MSD total energy	0	>.99		
MAP NGRad median	73.54	.26		
MAP QIV kurtosis	0.27	.27		
MAP QIV MAD	−0.02	>.99		
Combined model			0.88 (0.80, 0.96)	80 (57/71)
Intercept	−4.95	>.99		

Table 2 (continues)

Table 2 (continued): Logistic Regression Models in the Prediction of IDH and 1p/19q Genotype Grade II and III Gliomas

Model	β Level	Corrected <i>P</i> Value*	AUC [†]	Accuracy (%) [‡]
DTI AD interquartile range	−8.58	>.99		
DTI AD kurtosis	−0.20	>.99		
DKI AD skewness	−0.77	>.99		
DKI MD kurtosis	0.12	>.99		
DKI MD mean	−1.62	>.99		
NODDI ODI P90	16.06	.02		
MAP MSD energy	0	>.99		
MAP NGRad P10	24.96	>.99		
MAP QIV kurtosis	0.28	>.99		

Note.—*Intercept* refers to the value of the covariate when all independent variables are equal to 0. AD = axial diffusivity, AK = axial kurtosis, AUC = area under the receiver operating characteristic curve, DTI = diffusion-tensor imaging, DKI = diffusion-kurtosis imaging, FA = fractional anisotropy, ICVF = intracellular volume fraction, MAD = mean absolute deviation, MAP = mean apparent propagator, MD = mean diffusivity, MSD = mean squared displacement, NGRad = radial non-Gaussianity, NODDI = neurite orientation dispersion and density imaging, ODI = orientation dispersion index, P10 = 10th percentile, P90 = 90th percentile, QIV = q-space inverse variance, RD = radial diffusivity, RK = radial kurtosis, rMAD = robust mean absolute deviation, RMS = root mean squared, RTAP = return to the axis probability.

* *P* values were adjusted by Bonferroni correction for multiple comparisons.

[†] Data in parentheses are 95% CIs.

[‡] Data in parentheses are the numerator/denominator.

(Table E3 [online]). We found that the metrics histogram features that were useful for distinguishing the *IDH* genotype in LGG reflected non-Gaussian water diffusion, including the mean, 10th percentile, and root mean square mean kurtosis of DKI; the median, 10th percentile, and mean radial kurtosis of DKI; the root mean square, 90th percentile, and mean intracellular volume fraction of NODDI; the root mean square, 10th percentile, median, and mean axial non-Gaussianity of MAP; the root mean square, 10th percentile, 90th percentile, median, and mean radial non-Gaussianity of MAP; and the root mean square, 10th percentile, median, and mean non-Gaussianity of MAP.

Correlation of Diffusion MRI Metrics with Glioma Grade and the Ki-67 Labeling Index

Several histogram features can be found for all of the DTI, DKI, NODDI, and MAP metrics ($P < .001$) in identifying WHO grades II and III and especially in detecting WHO grades II and IV ($P < .001$). However, in identifying WHO grades III and IV, none of the metrics showed significant results ($P < .001$) (Table E3 [online]).

There were significant correlations between the Ki-67 labeling index and almost all the histogram features for the DTI, DKI, NODDI, and MAP metrics, but the correlation coefficients for all were less than 0.4. After multiple linear regression between the Ki-67 labeling index and the diffusion metrics histogram features, a model with R^2 of 0.844 ($P < .001$) was found to be the best, as illustrated in Table E4 (online).

There were many highly correlated (R absolute value greater than 0.75) diffusion metric pairs (Fig 6). For example, the return-to-the-plane probability of MAP was highly correlated

with the isotropic volume fraction of NODDI and the axial diffusivity, mean diffusivity, and radial diffusivity of DTI and DKI. However, the orientation dispersion index of NODDI showed weak or no correlation with all the other metrics (R absolute value less than 0.75).

Discussion

Exploration of an effective and noninvasive method for predicting glioma genotyping is important for individualized treatment and prognosis assessment of patients with glioma. Our results showed that the logistic regression model of whole-tumor histogram features of diffusion-tensor imaging, diffusion-kurtosis imaging, neurite orientation dispersion and density imaging, and mean apparent propagator, individually and in combination, showed no statistically significant differences in predicting glioma isocitrate dehydrogenase (*IDH*; minimum $P = .06$) or *1p/19q* (minimum $P = .11$) genotyping. Our results showed that any of the models (diffusion-tensor imaging, diffusion-kurtosis imaging, neurite orientation dispersion and density imaging, mean apparent propagator, and total diffusion models) could be individually used to predict *IDH* (area under the receiver operating characteristic curve [AUC], 0.76, 0.82, 0.78, 0.81, and 0.82, respectively) and *1p/19q* genotyping (AUC, 0.83, 0.81, 0.82, 0.83, and 0.88, respectively).

Similar to glioblastoma multiforme, LGG with wild-type *IDH* is more invasive than that with *IDH* mutations (1,3,21,22). Lower aggressiveness means lower cell-level protein and lower cell proliferation in the *IDH* mutation type versus the *IDH* wild-type (23,24), which could be detected with diffusion MRI metrics reflecting the microstructure at the cellular level (25,26). All the diffusion metrics could be

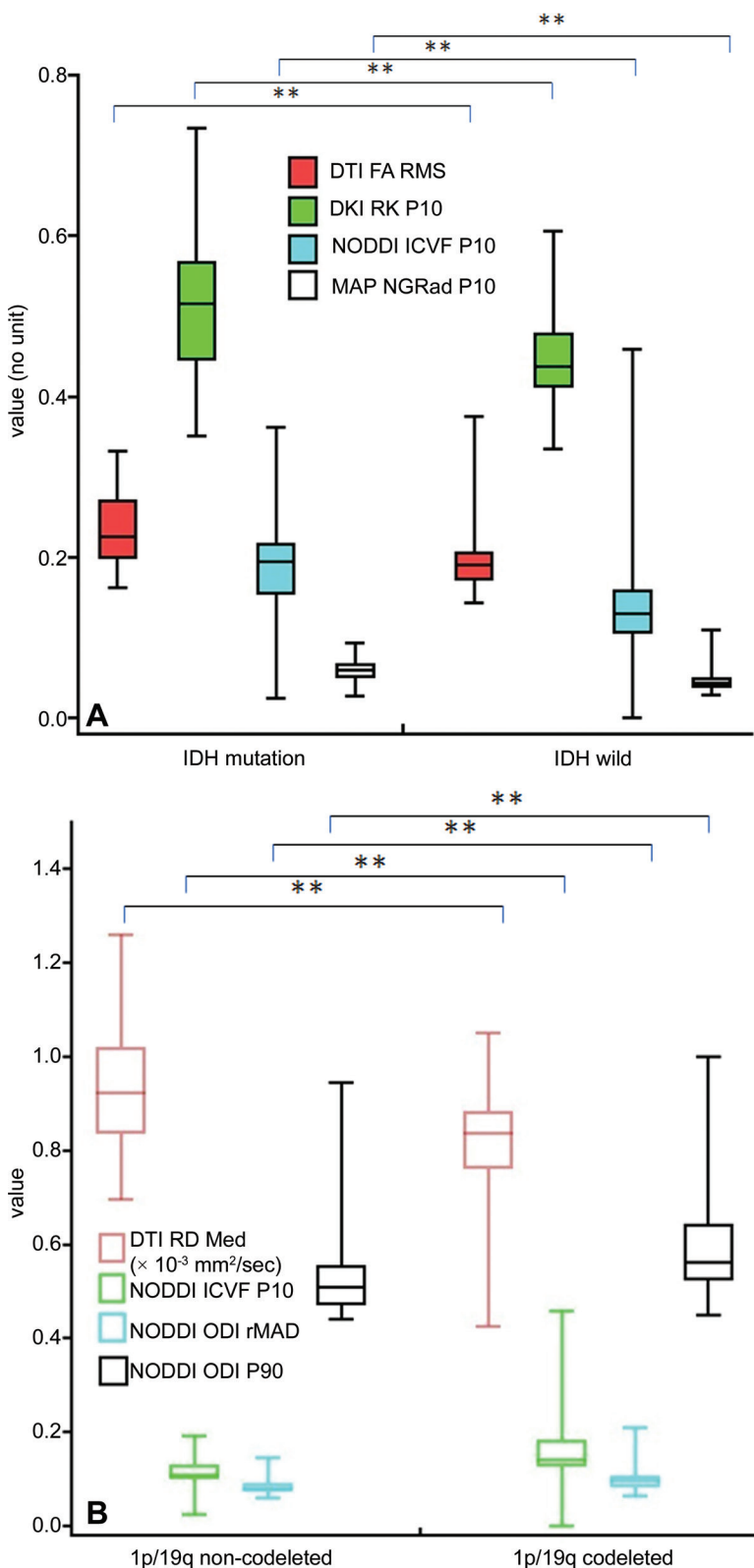


Figure 4: Plots show distribution of useful metrics for predicting (A) isocitrate dehydrogenase (IDH) mutation type in grade II and III glioma and predicting (B) 1p/19q codeletion in IDH mutation grade II and III glioma. DTI RMS = root mean square, FA = fractional anisotropy, DTI = diffusion-tensor imaging, DKI = diffusion-kurtosis imaging, ICVF = intracellular volume fraction, MAP = mean apparent propagator, med = median, NGRad = radial non-Gaussianity, NODDI = neurite orientation dispersion and density imaging, ODI = orientation dispersion index, P10 = 10th percentile, P90 = 90th percentile, RD = radial diffusivity, RK = radial kurtosis, rMAD = robust mean absolute deviation. ** $P < .001$.

used to detect *IDH* genotyping in LGG and glioblastoma multiforme simultaneously corresponding to non-Gaussian water diffusion in our study. Although the non-Gaussian metrics may also reflect the mixture of multiple tissue components, cellular density may have an important role here because the intracellular volume fraction (ICVF) from NODDI showed similar performance to the other non-Gaussian metrics; the 10th percentile ICVF histogram may reflect the status in the region without cellular structure and relate to tumor necrotic regions; compared with *IDH* wild-type, *IDH* mutations could cause inhibition of proliferation in glioma (24); and the value of NODDI ICVF in the cyst core was 0.

White matter tracts have been described (27–29) to exist in glioma tumors and peritumoral edema. When white matter is attacked, diffusion MRI metrics reflecting myelin integrity, such as ICVF and fractional anisotropy (29), will appear lower than normal white matter. The ICVF and fractional anisotropy were significantly lower in the LGG *IDH* mutation type than in the *IDH* wild-type. However, there was no significant difference in the mean value of orientation dispersion index from NODDI between the *IDH* wild-type and *IDH* mutation type LGG (0.358 vs 0.346, respectively; $P = .40$) in our study. Moreover, we noticed that the mean value of non-Gaussianity, axial non-Gaussianity, radial non-Gaussianity, return-to-the-axis probability, and return-to-the-origin probability from MAP were higher in *IDH* mutation type LGG than in *IDH* wild-type LGG in our study ($P < .001$). These MAP metrics are considered more powerful markers for demyelination than radial diffusivity and are well suited for characterizing complex diffusion in anisotropic tissues because they are determined by diffusion-tensor orientation and reveal additional information complementary to DTI and NODDI (30,31). Thus, non-Gaussianity, axial non-Gaussianity, radial non-Gaussianity, return-to-the-axis probability, and return-to-the-origin probability not only are useful metrics for clinical glioma *IDH* genotyping but also may be more precise markers for observing the microstructural changes in white matter fibers in glioma tumors and peritumoral edema.

Codeletion of 1p and 19q is another early genetic event of glioma closely related to the oligodendroglial lineage (32). 1p/19q non-codeletion gliomas are positively associated with cell division, extracellular matrix, and angiogenesis (33). Apparent diffusion coefficients have a negative correlation with cell proliferation, whereas the relative mean value of apparent diffusion coefficient was higher in 1p/19q non-codeletion than codeletion

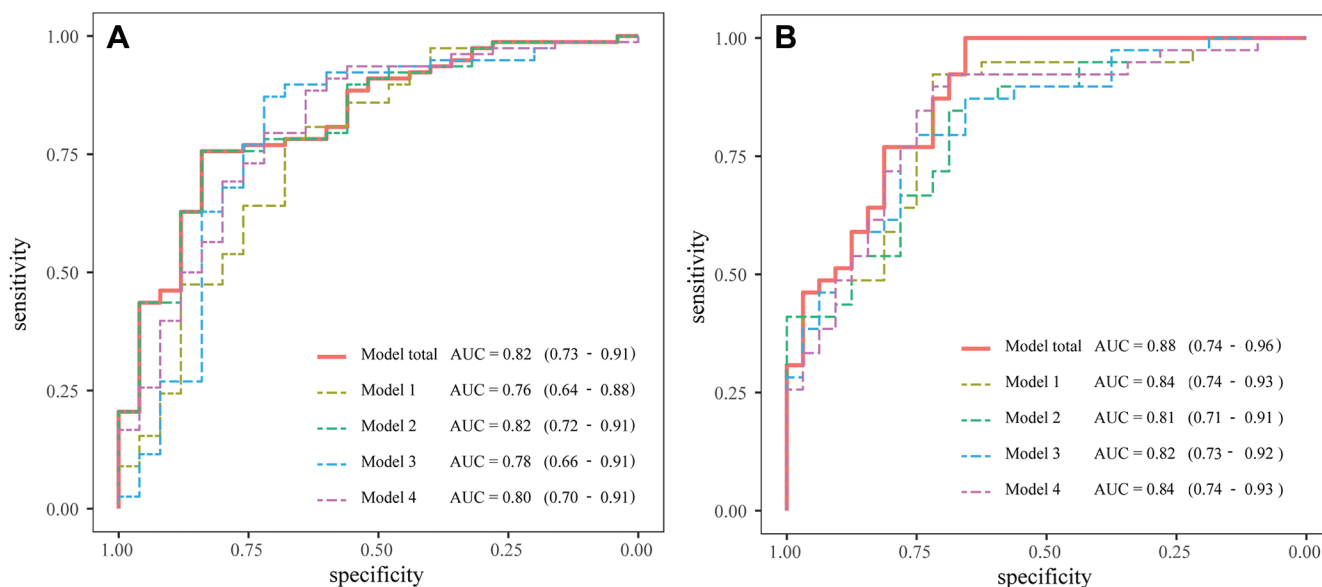


Figure 5: Areas under the receiver operating characteristic curve (AUCs) and 95% CIs (in parentheses) of diffusion-tensor imaging (model 1), diffusion-kurtosis imaging (model 2), neurite orientation dispersion and density imaging (model 3), and mean apparent propagator (model 4). The histogram logistical models predict **(A)** isocitrate dehydrogenase (*IDH*) mutation type in grade II and III glioma and **(B)** 1p/19q codeletion in *IDH* mutation glioma grade II and III.

Table 3: Comparison of the Logistic Regression Models in *IDH* and 1p/19q Genotyping of Grade II and III Gliomas

Parameter	<i>IDH</i> Mutant 1p/19q Genotype		<i>IDH</i> Genotype	
	McNemar Test	DeLong Test	McNemar Test	DeLong Test
Combined model vs DTI model	.72	.16	.45	.11
Combined model vs DKI model	.30	.06	>.99	.37
Combined model vs NODDI model	.18	.16	.50	.23
Combined model vs MAP model	.11	.17	.29	.29
DTI model vs DKI model	.61	.47	.29	.18
DTI model vs NODDI model	.45	.83	>.99	.64
DTI model vs MAP model	.2	.94	>.99	.38
DKI model vs NODDI model	>.99	.80	.34	.47
DKI model vs MAP model	>.99	.36	.18	.63
NODDI model vs MAP model	>.99	.82	>.99	.48

Note.—Data are *P* values; *P* values less than .05 indicate a statistically significant difference. McNemar test is for comparison of the difference of accuracy; DeLong test is for comparison of the difference of the area under the receiver operating characteristic curve. DKI = diffusion-kurtosis imaging, DTI = diffusion-tensor imaging, MAP = mean apparent propagator, NODDI = neurite orientation dispersion and density imaging.

IDH mutation type gliomas, and that in *IDH* wild-type gliomas is the lowest of all three glioma types (7,26). According to the results of the histogram analysis of the metrics, the median radial diffusivity of DTI showed the same distribution trend as the relative mean value of the apparent diffusion coefficient in the three groups, and the mean ICVF showed the inverse distribution trend with the relative mean value of the apparent diffusion coefficient. Therefore, ICVF is a promising metric for clinical glioma 1p/19q genotyping, and there may be an unclear mechanism by which 1p/19q genotyping influences cell proliferation in *IDH*-mutated LGG.

NODDI and MAP provide more significant information regarding the tumor microstructure than DTI and DKI

because they include metrics reflecting the intracellular volume and white matter demyelination. However, these advantages are on the basis of technical principles and indirect results, without the direct pathologic basis of point-by-point results, indicating the necessity for further research.

Our study had limitations. First, a larger sample size is needed to verify the results of predicting 1p/19q codeletion. Moreover, image features such as calcification (34) and T2-weighted fluid-attenuated inversion recovery mismatch (35), which may improve the effectiveness of the predictive model, were not included in our study.

In conclusion, whole-tumor histogram analysis of multiple diffusion metrics is a promising approach for glioma isocitrate

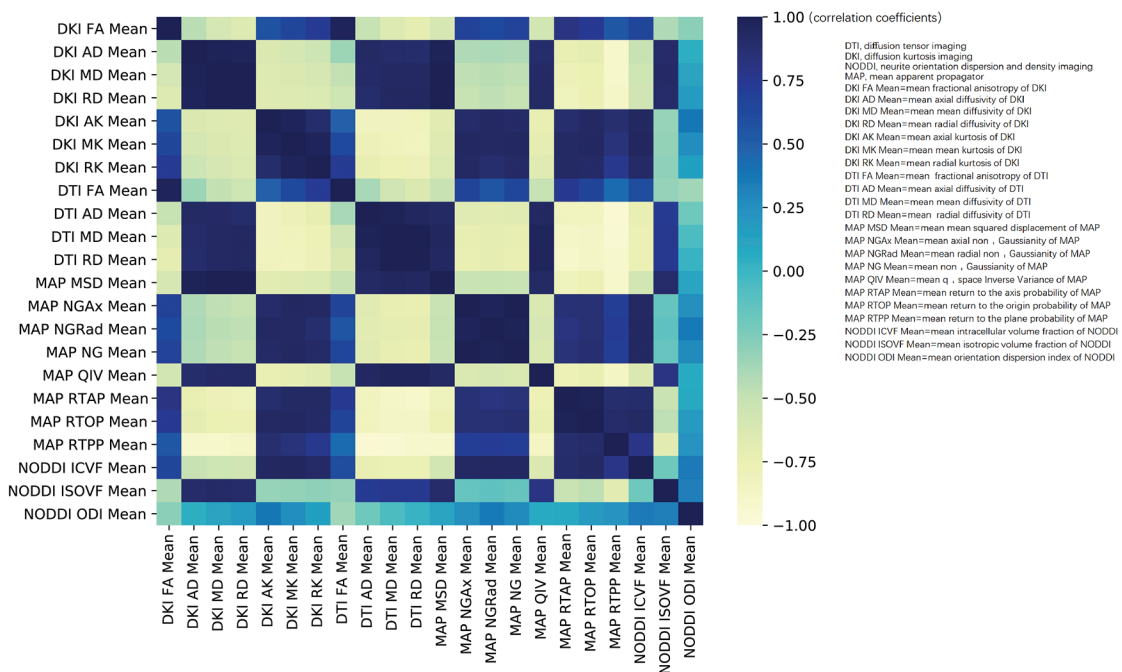
Table 4: Performance of Diffusion MRI Metrics in the Genotyping of IDH and 1p/19q in Grade II and III Gliomas

Parameter	IDH Genotyping					IDH Mutation 1p/19q Genotyping		
	DTI FA RMS	DKI RK P10	NODDI ICVF P10	MAP NGRad P10	DTI RD Median	NODDI ICVF P10	NODDI ODI rMAD	NODDI ODI P90
AUC*	0.74 (0.62, 0.86)	0.75 (0.63, 0.87)	0.79 (0.68, 0.91)	0.78 (0.66, 0.90)	0.76 (0.65, 0.87)	0.78 (0.67, 0.88)	0.71 (0.59, 0.83)	0.74 (0.62, 0.85)
Accuracy (%)	80 (82/103)	79 (81/103)	79 (81/103)	82 (84/103)	72 (55/76)	76 (58/76)	64 (49/76)	68 (52/76)
Sensitivity (%)	97 (76/78)	96 (75/78)	99 (77/78)	97 (76/78)	63 (22/35)	74 (26/35)	63 (22/35)	66 (23/35)
Specificity (%)	24 (6/25)	24 (6/25)	16 (4/25)	32 (8/25)	81 (33/41)	78 (32/41)	66 (27/41)	71 (29/41)
Optimal threshold	0.26	0.49	0.17	0.05	0.90 [†]	0.12	0.09	0.52

Note.—Data in parentheses are the numerator/denominator of participants included for each parameter, unless otherwise indicated. Values correspond to the optimal threshold according to the Youden index. AUC = area under the receiver operating characteristic curve, DTI = diffusion-tensor imaging, DKI = diffusion-kurtosis imaging, FA = fractional anisotropy, ICVF = intracellular volume fraction, IDH = isocitrate dehydrogenase, MAP = mean apparent propagator, NGRad = radial non-Gaussianity, NODDI = neurite orientation dispersion and density imaging, ODI = orientation dispersion index, P10 = 10th percentile, P90 = 90th percentile, RD = radial diffusivity, RK = radial kurtosis, rMAD = robust mean absolute deviation, RMS = root mean squared.

* Data in parentheses are 95% CIs.

[†] $\times 10^{-3}$ mm²/sec.

**Figure 6:** Heat map of correlations between the diffusion metrics.

dehydrogenase (IDH) and 1p/19q genotyping; there was similar satisfactory performance among the diffusion models, both individually and in combination for predicting glioma IDH and 1p/19q genotyping.

Acknowledgment: The authors thank Chunhua Song, PhD, who provided valuable assistance with the statistical analysis.

Author contributions: Guarantors of integrity of entire study, A.G., J.C.; study concepts/study design or data acquisition or data analysis/interpretation, all authors; man-

uscript drafting or manuscript revision for important intellectual content, all authors; approval of final version of submitted manuscript, all authors; agrees to ensure any questions related to the work are appropriately resolved, all authors; literature research, A.G., H.Z., J.Q., J.B., Y.Z., J.C.; clinical studies, A.G., S.W., Q.C., E.G., J.Q., J.B., Y.Z., J.C.; experimental studies, A.G., X.Y., S.W., J.Q., J.B.; statistical analysis, A.G., J.C.; and manuscript editing, A.G., H.Z., X.Y., S.W., Y.Z., J.C.

Disclosures of conflicts of interest: A.G. No relevant relationships. H.Z. Employed by Siemens Healthineers. X.Y. Employed by Siemens Healthineers. S.W. Employed by Siemens Healthineers. Q.C. No relevant relationships. E.G. No relevant relationships. J.Q. No relevant relationships. J.B. No relevant relationships. Y.Z. No relevant relationships. J.C. No relevant relationships.

References

- Louis DN, Perry A, Reifenberger G, et al. The 2016 World Health Organization Classification of Tumors of the Central Nervous System: a summary. *Acta Neuropathol (Berl)* 2016;131(6):803–820.
- Eckel-Passow JE, Lachance DH, Molinaro AM, et al. Glioma Groups Based on 1p/19q, *IDH*, and TERT Promoter Mutations in Tumors. *N Engl J Med* 2015;372(26):2499–2508.
- Cancer Genome Atlas Research Network; Brat DJ, Verhaak RG, et al. Comprehensive, Integrative Genomic Analysis of Diffuse Lower-Grade Gliomas. *N Engl J Med* 2015;372(26):2481–2498.
- Le Rhun E, Taillibert S, Chamberlain MC. Current Management of Adult Diffuse Infiltrative Low Grade Gliomas. *Curr Neurol Neurosci Rep* 2016;16(2):15.
- Duffau H, Taillandier L. New concepts in the management of diffuse low-grade glioma: Proposal of a multistage and individualized therapeutic approach. *Neuro Oncol* 2015;17(3):332–342.
- Park CJ, Choi YS, Park YW, et al. Diffusion tensor imaging radiomics in lower-grade glioma: improving subtyping of isocitrate dehydrogenase mutation status. *Neuroradiology* 2020;62(3):319–326.
- Maynard J, Okuchi S, Wastling S, et al. World Health Organization Grade II/III Glioma Molecular Status: Prediction by MRI Morphologic Features and Apparent Diffusion Coefficient. *Radiology* 2020;296(1):111–121. [Published correction appears in *Radiology* 2021;298(1):E61.]
- Zhang HW, Lyu GW, He WJ, et al. DSC and DCE Histogram Analyses of Glioma Biomarkers, Including *IDH*, MGMT, and TERT, on Differentiation and Survival. *Acad Radiol* 2020;27(12):e263–e271.
- Figini M, Riva M, Graham M, et al. Prediction of Isocitrate Dehydrogenase Genotype in Brain Gliomas with MRI: Single-Shell versus Multishell Diffusion Models. *Radiology* 2018;289(3):788–796.
- Ozturk-Isik E, Cengiz S, Ozcan A, et al. Identification of IDH and TERTp mutation status using ¹H-MRS in 112 hemispheric diffuse gliomas. *J Magn Reson Imaging* 2020;51(6):1799–1809.
- Xing Z, Yang X, She D, Lin Y, Zhang Y, Cao D. Noninvasive Assessment of *IDH* Mutational Status in World Health Organization Grade II and III Astrocytomas Using DWI and DSC-PWI Combined with Conventional MR Imaging. *AJNR Am J Neuroradiol* 2017;38(6):1138–1144.
- Xiong J, Tan W, Wen J, et al. Combination of diffusion tensor imaging and conventional MRI correlates with isocitrate dehydrogenase 1/2 mutations but not 1p/19q genotyping in oligodendroglial tumours. *Eur Radiol* 2016;26(6):1705–1715.
- Hempel JM, Bisdas S, Schittenhelm J, et al. In vivo molecular profiling of human glioma using diffusion kurtosis imaging. *J Neurooncol* 2017;131(1):93–101. [Published correction appears in *J Neurooncol* 2017;131(1):103.]
- Zhao J, Wang YL, Li XB, et al. Comparative analysis of the diffusion kurtosis imaging and diffusion tensor imaging in grading gliomas, predicting tumour cell proliferation and *IDH-1* gene mutation status. *J Neurooncol* 2019;141(1):195–203.
- Zhao J, Li JB, Wang JY, et al. Quantitative analysis of neurite orientation dispersion and density imaging in grading gliomas and detecting *IDH-1* gene mutation status. *Neuroimage Clin* 2018;19:174–181.
- Aliotta E, Nourzadeh H, Batchala PP, et al. Molecular Subtype Classification in Lower-Grade Glioma with Accelerated DTI. *AJNR Am J Neuroradiol* 2019;40(9):1458–1463.
- Özarslan E, Koay CG, Shepherd TM, et al. Mean apparent propagator (MAP) MRI: a novel diffusion imaging method for mapping tissue microstructure. *Neuroimage* 2013;78:16–32.
- Fick RHJ, Wassermann D, Caruyer E, Deriche R. MAPL: Tissue microstructure estimation using Laplacian-regularized MAP-MRI and its application to HCP data. *Neuroimage* 2016;134:365–385.
- Wang P, Weng L, Xie S, et al. Primary application of mean apparent propagator-MRI diffusion model in the grading of diffuse glioma. *Eur J Radiol* 2021;138:109622.
- Daducci A, Canales-Rodríguez EJ, Zhang H, Dyrby TB, Alexander DC, Thiran JP. Accelerated Microstructure Imaging via Convex Optimization (AMICO) from diffusion MRI data. *Neuroimage* 2015;105:32–44.
- Price SJ, Allinson K, Liu H, et al. Less Invasive Phenotype Found in Isocitrate Dehydrogenase-mutated Glioblastomas than in Isocitrate Dehydrogenase Wild-Type Glioblastomas: A Diffusion-Tensor Imaging Study. *Radiology* 2017;283(1):215–221.
- Chen R, Smith-Cohn M, Cohen AL, Colman H. Glioma Subclassifications and Their Clinical Significance. *Neurotherapeutics* 2017;14(2):284–297.
- Berens ME, Sood A, Barnholtz-Sloan JS, et al. Multiscale, multimodal analysis of tumor heterogeneity in *IDH1* mutant vs wild-type diffuse gliomas. *PLoS One* 2019;14(12):e0219724.
- Bralten LB, Kloosterhof NK, Balvers R, et al. *IDH1 R132H* decreases proliferation of glioma cell lines in vitro and in vivo. *Ann Neurol* 2011;69(3):455–463.
- Xiong J, Tan WL, Pan JW, et al. Detecting isocitrate dehydrogenase gene mutations in oligodendroglial tumors using diffusion tensor imaging metrics and their correlations with proliferation and microvascular density. *J Magn Reson Imaging* 2016;43(1):45–54.
- Wu CC, Jain R, Radmanesh A, et al. Predicting Genotype and Survival in Glioma Using Standard Clinical MR Imaging Apparent Diffusion Coefficient Images: A Pilot Study from The Cancer Genome Atlas. *AJNR Am J Neuroradiol* 2018;39(10):1814–1820.
- Seow P, Hernowo AT, Narayanan V, et al. Neural Fiber Integrity in High-Versus Low-Grade Glioma using Probabilistic Fiber Tracking. *Acad Radiol* 2020. 10.1016/j.acra.2020.09.007. Published online October 3, 2020.
- Barajas RF Jr, Hess CP, Phillips JJ, et al. Super-resolution track density imaging of glioblastoma: histopathologic correlation. *AJNR Am J Neuroradiol* 2013;34(7):1319–1325.
- Stikov N, Campbell JS, Stroh T, et al. In vivo histology of the myelin g-ratio with magnetic resonance imaging. *Neuroimage* 2015;118:397–405.
- Maximov II, Tonoyan AS, Pronin IN. Differentiation of glioma malignancy grade using diffusion MRI. *Phys Med* 2017;40:24–32.
- Avram AV, Sarlls JE, Barnett AS, et al. Clinical feasibility of using mean apparent propagator (MAP) MRI to characterize brain tissue microstructure. *Neuroimage* 2016;127:422–434.
- Riemenschneider MJ, Jeuken JW, Wesseling P, Reifenberger G. Molecular diagnostics of gliomas: state of the art. *Acta Neuropathol (Berl)* 2010;120(5):567–584.
- Chai RC, Zhang KN, Chang YZ, et al. Systematically characterize the clinical and biological significances of 1p19q genes in 1p/19q non-codeletion glioma. *Carcinogenesis* 2019;40(10):1229–1239.
- Yamauchi T, Ohno M, Matsushita Y, et al. Radiological characteristics based on isocitrate dehydrogenase mutations and 1p/19q codeletion in grade II and III gliomas. *Brain Tumor Pathol* 2018;35(3):148–158.
- Jain R, Johnson DR, Patel SH, et al. “Real world” use of a highly reliable imaging sign: “T2-FLAIR mismatch” for identification of *IDH* mutant astrocytomas. *Neuro Oncol* 2020;22(7):936–943.

Erratum

Originally published in:

<https://doi.org/10.1148/radiol.210820>

Whole-Tumor Histogram Analysis of Multiple Diffusion Metrics for Glioma Genotyping

Ankang Gao, Huiting Zhang, Xu Yan, Shaoyu Wang, Qianqian Chen, Eryuan Gao, Jinbo Qi, Jie Bai, Yong Zhang, Jingliang Cheng

Erratum in:

<https://doi.org/10.1148/radiol.219034>

The affiliations contained an error and has been changed to Siemens **Healthineers**; Figure 4B contained an error and has been corrected to $\times 10^{-3} \text{ mm}^2/\text{sec}$.

Erratum

Originally published in:

<https://doi.org/10.1148/radiol.210820>

Whole-Tumor Histogram Analysis of Multiple Diffusion Metrics for Glioma Genotyping

Ankang Gao, Huiting Zhang, Xu Yan, Shaoyu Wang, Qianqian Chen, Eryuan Gao, Jinbo Qi, Jie Bai, Yong Zhang, Jingliang Cheng

Erratum in:

<https://doi.org/10.1148/radiol.219034>

The affiliations contained an error and has been changed to Siemens **Healthineers**; Figure 4B contained an error and has been corrected to $\times 10^{-3} \text{ mm}^2/\text{sec}$.